

High mobility two-dimensional hole system on hydrogen-terminated silicon (111) surfaces

Binhui Hu,^{a)} Tomasz M. Kott, Robert N. McFarland,^{b)} and B. E. Kane

Laboratory for Physical Sciences, University of Maryland at College Park, College Park, MD 20740

(Dated: 19 January 2012)

We have realized a two-dimensional hole system (2DHS), in which the 2DHS is induced at an atomically flat hydrogen-terminated Si(111) surface by a negative gate voltage applied across a vacuum cavity. Hole densities up to $7.5 \times 10^{11} \text{ cm}^{-2}$ are obtained, and the peak hole mobility is about $10^4 \text{ cm}^2/\text{Vs}$ at 70 mK. The quantum Hall effect is observed. Shubnikov-de Haas oscillations show a beating pattern due to the spin-orbit effects, and the inferred zero-field spin splitting can be tuned by the gate voltage.

Metal-oxide-semiconductor (MOS) field-effect transistors (FETs) have long been used to study two-dimensional systems in silicon. While there has been extensive research on two-dimensional electron systems (2DESs) in silicon using MOSFETs over the last several decades,^{1,2} comparably little work has been done on two-dimensional hole systems (2DHSs),²⁻⁵ primarily due to the fact that holes have lower mobility than electrons, and detailed study was not possible at such low mobility silicon hole devices.

Recently, a new type of silicon FET device has been developed, in which an atomically flat silicon (111) surface is terminated by a monolayer of hydrogen atoms, and a 2DES is induced at the H-Si(111) surface by a positive gate voltage through a vacuum barrier.⁶ 2DESs in these vacuum FET devices show extremely high mobility.⁶⁻⁸ In this letter, we report that the vacuum FET technique can be extended to 2DHSs. A peak hole mobility of $\sim 10^4 \text{ cm}^2/\text{Vs}$ is obtained, exceeding by one order of magnitude the mobility in MOS structures and comparable with the mobility of pseudomorphic Si/SiGe heterostructures,^{9,10} where 2DHSs reside in the SiGe channels. The integer quantum Hall effect (IQHE) is also observed. At lower magnetic fields, Shubnikov-de Haas (SdH) oscillations show a beating pattern, which is due to the zero-field spin splitting.¹¹ In silicon, the spin-orbit effects lift the spin-degeneracy of the heavy hole subband even in a zero external magnetic field. The zero-field spin splitting is from the structure inversion asymmetry (SIA),¹² and can be tuned by the external gate. The zero-field spin splitting is of great interest because of its potential use in spintronics devices¹³ and in studying fundamental physics.¹²

The vacuum FET device includes two pieces, as shown in Fig. 1. One is a p^- Si(111) piece (float zone, resistance $> 10000 \Omega\text{-cm}$), and the other is a silicon-on-insulator (SOI) piece. First, four p^+ contact regions are formed in the Si(111) piece by ion implantation with 2.4×10^{15}

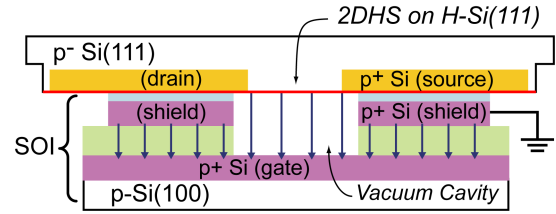


FIG. 1. (Color online) Schematic cross section of a vacuum FET (not to scale). A H-Si(111) piece is contact bonded to a SOI piece in a vacuum. The H-Si(111) piece has heavily boron-doped (p^+) regions to make contact to the 2DHS. In the SOI piece, the shield and the gate are p^+ layers formed by double boron ion implantation. Dry etching is used to create the cavity. The arrows depict the electric field. The 2DHS is induced at the H-Si(111) surface in the encapsulated vacuum cavity.

cm^{-2} , 15 keV boron ions through a 30 nm thick thermal oxide, as shown in the insert of Fig. 2. It is annealed in N_2 gas at 1000°C for 10 minutes to activate dopants and reduce defects. Second, in the SOI piece, the shield and gate conducting layers are formed by double boron ion implantation, and a cloverleaf-shaped cavity is created by dry etching. Finally, the Si(111) piece is H-terminated by immersing it in an ammonium fluoride solution, and then these two pieces are contact bonded in a vacuum chamber. The detailed fabrication processes and the basic operating principle have been discussed elsewhere.^{6,14} Here the SOI piece acts as a remote gate to induce a 2DHS at the Si(111) surface through the encapsulated vacuum cavity. This cavity also protects the air sensitive H-Si(111) surface. Compared to the Si/SiO₂ interface in MOSFETs, the vacuum/H-Si(111) interface is atomically flat and has much fewer defects, leading to a much higher carrier mobility.

The devices are characterized in a dilution refrigerator with a base temperature of $\sim 70 \text{ mK}$. Longitudinal (R_{xx}) and Hall (R_{xy}) resistances are determined by Van der Pauw measurements with the standard low-frequency AC lock-in technique using a 7 Hz, 100 nA current source. As shown in the insert of Fig. 2, the Van der Pauw geometry consists of a center cloverleaf-shaped 2DHS, which is electric field induced, and four heavily boron-doped con-

^{a)}To whom correspondence should be addressed. Electronic mail: hubh@lps.umd.edu

^{b)}Present address: iSW, Arlington, VA 22203, USA.

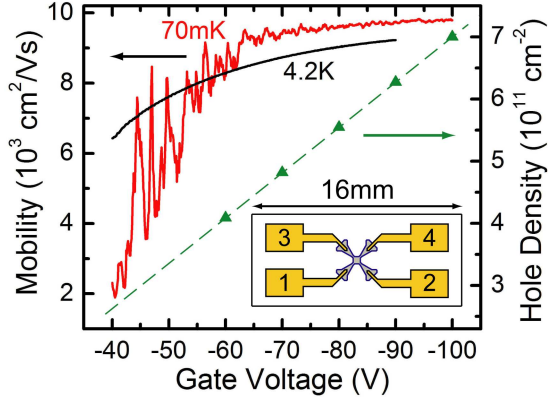


FIG. 2. (Color online) Left axis: mobility as a function of gate voltage at 70 mK and 4.2 K. At 70 mK, the wild fluctuations of the mobility are due to the high contact resistances to the 2DHS. Right axis: Hole density vs gate voltage. The hole densities (triangles) are determined by the magnetic field B at the filling factor $\nu = 5$ minima: $p_{2d} = \nu e B / h$. The dashed line is a linear fit. Insert: on the Si(111) piece, Van der Pauw geometry consists of a cloverleaf-shaped 2DHS with a 0.5×0.5 mm² center square, and four heavily boron-doped contacts.

tacts (labeled as 1, 2, 3, 4). Four-terminal resistance is defined as $R_{ij,lm} = V_{lm} / I_{ij}$ ($i, j, l, m = 1, 2, 3, 4$), where current I_{ij} is fed from contact i to contact j , and voltage V_{lm} is measured between contacts l and m . The sheet resistance is determined by the standard Van der Pauw technique.¹⁵ Although the Van der Pauw geometry is symmetric, R_{xx} and R_{yy} are found to differ by $\sim 35\%$, so the sheet resistance, as well as the mobility, is the average of x and y directions.¹⁶ The anisotropy can be caused by some mechanisms such as miscut, disorder, strain and the non-parabolicity of the valence band,^{7,8,17} but the exact sources are yet to be ascertained. Hole density p_{2d} is determined by the magnetic field B at the filling factor $\nu = 5$ minimum of the longitudinal resistance curve at $T \sim 1$ K: $p_{2d} = \nu e B / h$, where e is the electron charge and h is Planck's constant. The data (triangles) are shown in Fig. 2, and the dashed line is a linear fit. Hole densities up to 7.5×10^{11} cm⁻² ($V_g = -110$ V) are obtained. If we use a parallel plate capacitor model, the equivalent depth of the cavity is 759 nm, which is consistent with the measurement result from a profilometer. The extrapolated threshold voltage is -3.9 V, which indicates the density of the trapped charge at the surface $\sim 2.8 \times 10^{10}$ cm⁻². The mobility of the 2DHS is also shown in Fig. 2, and the peak mobility is about 9800 cm²/Vs at gate voltage $V_g = -100$ V, $T = 70$ mK on this device. This is one order of magnitude higher than the hole mobility of a Si(111) MOSFET.⁴ The contact resistances between the contacts and the 2DHS increase dramatically at $|V_g| < 60$ V, when the temperature is lowered from 4.2 K to 70 mK. For example, they increase from ~ 20 K Ω to ~ 400 K Ω at $V_g = -50$ V. It is difficult to get reliable measurements at this region, and the calculated mobility shows spurious wild fluctuations at $T = 70$ mK. Our discussion

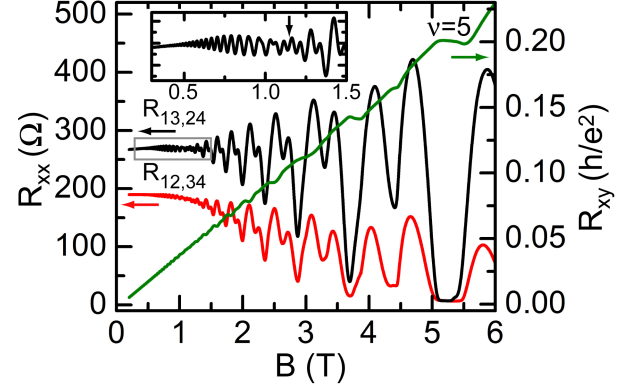


FIG. 3. (Color online) Longitudinal resistances $R_{13,24}$, $R_{12,34}$, and Hall resistance R_{xy} vs perpendicular magnetic field B at $V_g = -90$ V ($p_{2d} = 6.27 \times 10^{11}$ cm⁻²) and $T = 70$ mK. Quantum Hall effect is observed near $B = 5.2$ T. The insert shows an enlarged section of $R_{13,24}$, which exhibits a beating pattern, and the arrow marks the node location ($B = 1.14$ T).

below will focus on the data at $|V_g| > 60$ V.

As evidence of the high mobility 2DHS, Fig. 3 shows the longitudinal (R_{xx}) and Hall (R_{xy}) resistances as a function of perpendicular magnetic field B at $V_g = -90$ V ($p_{2d} = 6.27 \times 10^{11}$ cm⁻²) and $T = 70$ mK. The integer quantum Hall effect (IQHE) is observed. At the vicinity of $B = 5.2$ T, R_{xx} approaches zero, and R_{xy} develops a plateau at $\nu = 5$. Clear SdH oscillations appear at B field above 0.4 T. A close look at the trace of R_{xx} reveals a beating pattern of the SdH oscillations with a node near $B = 1.2$ T, as shown in the insert of Fig. 3. Although the beating pattern has been observed in p-channel Si(110) devices,^{3,5} to our best knowledge, this is the first time it has been observed on a Si(111) surface. The beating pattern can be explained by the spin-orbit effects, although different explanations exist. It could be from gross inhomogeneities of the carrier density in the sample.¹⁸ Two samples from different wafers have been measured, and both show a similar beating pattern. At $V_g = -90$ V, the beating node is located at $B = 1.14$ T for the device reported here, and it is at $B = 1.17$ T for the other device. It is therefore highly unlikely that the gross inhomogeneities are the cause.

The beating pattern indicates that there are two closely spaced frequency components with similar amplitudes, arising from two populations of holes. The hole subband densities p_{2d}^+ and p_{2d}^- can be determined by the Fourier analysis of the SdH oscillations with $p_{2d}^\pm = g_s e f^\pm / h$, where g_s is the degeneracy factor, f^+ and f^- are the frequencies of the SdH oscillations (Fig. 4(b)).^{19,20} Here R_{xx} vs B^{-1} data in the range $0.2 < B < 4$ T are Fourier transformed after subtraction of a slowly varying background, and peak locations are used as the frequencies of the SdH oscillations. For $|V_g| \geq 85$ V (with two well-resolved peaks), g_s must be 1 in order to have the sum of the subband densities equal to the

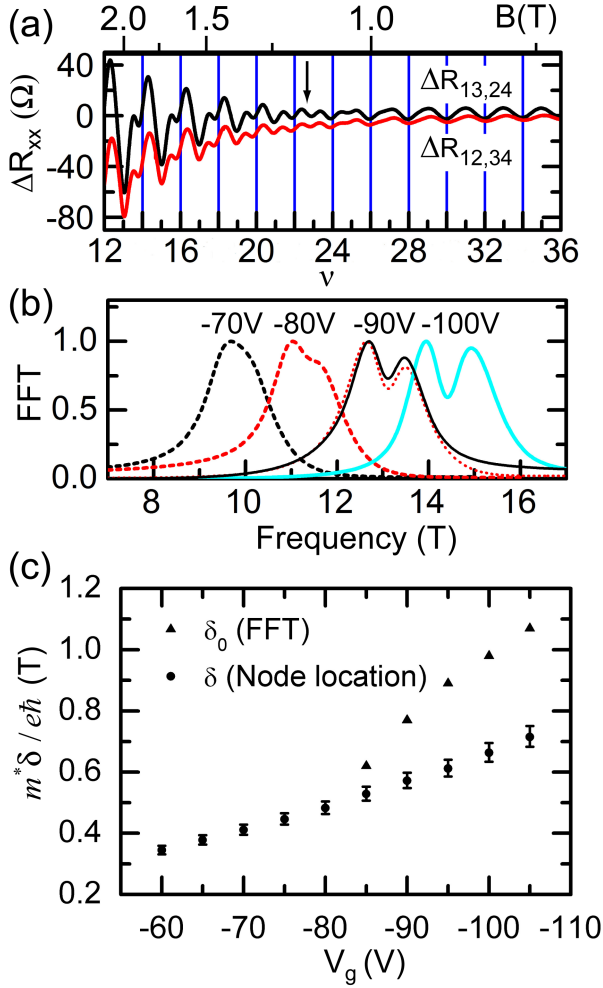


FIG. 4. (Color online) (a) $\Delta R_{13,24}(=R_{13,24}(B)-R_{13,24}(0))$, $\Delta R_{12,34}(=R_{12,34}(B)-R_{12,34}(0))$ vs filling factor ν at $V_g = -90$ V and $T = 70$ mK. The corresponding magnetic field B is shown on the top axis. The node location ($B = 1.14$ T) is marked by an arrow. Across the node, the minima change from the odd numbers of ν to the even numbers of ν . (b) Fourier power spectra of the SdH oscillations ($R_{13,24}$) at different gate voltages. Maximum peak amplitudes are normalized to 1. At $V_g = -90$ V, the solid line is the power spectrum of $R_{13,24}$, and the dotted line is the power spectrum of $R_{12,34}$. (c) Zero-field spin splitting and total spin splitting (both divided by $e\hbar/m^*$) vs gate voltage. Zero-field spin splitting is determined by Fourier power spectrum (b). The total spin splitting is determined by the node location (a), and the error bars are estimated by the error bound $[\nu_{node}-1, \nu_{node}+1]$, where ν_{node} is the node location in terms of filling factor.

total density, so these two components can only be from one subband with two spin-split levels, i.e. two spin-split subbands.

Landau levels of each spin population give rise to magnetoresistance oscillations with similar amplitude, described by $\cos[2\pi(E_f \pm \delta/2)/\hbar\omega_c]$, where E_f is the Fermi energy, δ is the energy separation between the two spin-split subbands, \hbar is $h/2\pi$, and ω_c is the cy-

clotron frequency.¹¹ The sum of these two components leads to the modulation of the SdH oscillations given by $A \sim \cos(\pi\delta/\hbar\omega_c)$. Beating nodes are located at $\delta/\hbar\omega_c = n = \pm 0.5, \pm 1.5$, etc. Only one node is clearly identified near $B \sim 1.2$ T (Fig. 3). Fig. 4(a) shows the SdH oscillations in terms of filling factor ν at $V_g = -90$ V. At $\nu < 22.7$, the minima of the SdH oscillations are at the odd numbers of ν . At $\nu > 22.7$, the minima are at the even numbers of ν . This manifests the transition across the node. We assume that the node corresponds to $n = 0.5$ (highest-field), because the $n = 0.5$ node is most easily observed, and there is no other node up to 6 T.¹³ The $n = 1.5$ node is estimated to be around $B \sim 0.4$ T, one third of the $n = 0.5$ node, so it is difficult to observe for this device. From the node location B_{node} , the total spin splitting can be determined by $\delta = 0.5\hbar\omega_c = (e\hbar/m^*)(0.5B_{node})$, where m^* is the effective hole mass. In Fig. 4(c), the total spin splitting δ is described by $m^*\delta/e\hbar = 0.5B_{node}$.

In theories of the spin-orbit interaction, spin splitting can have complicated B dependence.¹² The total spin splitting δ can be expanded as $\delta = \delta_0 + \delta_1(\hbar\omega_c) + \delta_2(\hbar\omega_c)^2 + \dots$, where δ_0 is the zero-field spin splitting, $\delta_1(\hbar\omega_c)$ is the linear splitting, etc.¹¹ For low magnetic fields, if only the first two terms are considered, then $A \sim \cos(\pi\delta_0/\hbar\omega_c + \pi\delta_1)$. The frequencies f^\pm of the SdH oscillations can be used to determine the zero-field spin splitting by $\delta_0 = (e\hbar/m^*)(f^+ - f^-)$. So the zero-field spin splitting δ_0 can be described by $m^*\delta_0/e\hbar = f^+ - f^-$, also shown in Fig. 4(c). There are two important features in the data. First, the zero-field spin splitting increases with increasing perpendicular electric field E_z . Second, at $|V_g| \geq 85$ V, $\delta_0 > \delta$, which means that a perpendicular magnetic field can *reduce* the spin splitting. More detailed analysis is needed to better appreciate the results. These topics will be explored in future studies.

In conclusion, the vacuum FET technique has been demonstrated to create high mobility 2DHSs in Si(111). In these high mobility 2DHSs, we are able to observe the IQHE, and the beating pattern of the SdH oscillations on Si(111) surfaces, which are difficult to reach previously. There are many interesting questions yet to be resolved, such as the non-parabolic valence band structure and the spin-orbit effects. Our high mobility 2DHSs open up new opportunities to explore fundamental physics in the two-dimensional hole systems. In addition, with the ability to create both a 2DES and a 2DHS on a Si(111) surface, it is straightforward to develop a bipolar surface device.

This work was funded by the Laboratory for Physical Sciences. The authors are grateful to Oney Soykal, Charles Tahan, Kevin Eng, and Kei Takashina for insightful discussions and technical help.

¹K. von Klitzing, G. Dorda, and M. Pepper, Phys. Rev. Lett. **45**, 494 (1980).

²T. Ando, A. B. Fowler, and F. Stern, Rev. Mod. Phys. **54**, 437 (1982), and references therein.

³K. von Klitzing, G. Landwehr, and G. Dorda, Solid State Commun. **14**, 387 (1974).

- ⁴K. von Klitzing, G. Landwehr, and G. Dorda, Solid State Commun. **15**, 489 (1974).
- ⁵S. I. Dorozhkin and E. B. Ol'shanetskiĭ, Pis'ma Zh. Eksp. Teor. Fiz. **46**, 399 (1987) [JETP Lett. **46**, 502 (1987)]
- ⁶K. Eng, R. N. McFarland, and B. E. Kane, Appl. Phys. Lett. **87**, 052106 (2005).
- ⁷K. Eng, R. N. McFarland, and B. E. Kane, Phys. Rev. Lett. **99**, 016801 (2007).
- ⁸R. N. McFarland, T. M. Kott, L. Sun, K. Eng, and B. E. Kane, Phys. Rev. B **80**, 161310 (2009).
- ⁹T. E. Whall, A. D. Plews, N. L. Matthey, and E. H. C. Parker, Appl. Phys. Lett. **65**, 3362 (1994); E. Basaran, R. A. Kubiak, T. E. Whall, and E. H. C. Parker, *ibid.* **64**, 3470 (1994).
- ¹⁰Strained Ge channels on SiGe virtual substrates can reach a higher hole mobility of $\sim 120000 \text{ cm}^2/\text{Vs}$ at 2 K, as shown in B. Rössner, D. Chrastina, G. Isella, and H. von Känel, Appl. Phys. Lett. **84**, 3058 (2004).
- ¹¹W. Zawadzki and P. Pfeffer, Semicond. Sci. Technol. **19**, R1 (2004).
- ¹²R. Winkler, *Spin-orbit Coupling Effects in Two-Dimensional Electron and Hole Systems* (Springer, Berlin, 2003).
- ¹³S. Datta and B. Das, Appl. Phys. Lett. **56**, 665 (1990).
- ¹⁴R. N. McFarland, *Multi-Valley Physics of Two-Dimensional Electron Systems on Hydrogen-Terminated Silicon (111) Surfaces*, PhD dissertation, University of Maryland, Department of Physics (2010).
- ¹⁵L. T. van der Pauw, Philips Res. Rep. **13**, 1 (1958).
- ¹⁶O. Bierwagen, R. Pomraenke, S. Eilers, and W. T. Masselink, Phys. Rev. B **70**, 165307 (2004).
- ¹⁷F. J. Ohkawa and Y. Uemura, Prog. Theor. Phys. Suppl. **57**, 164 (1975).
- ¹⁸B. L. Booth and A. W. Ewald, Phys. Rev. **168**, 796 (1968).
- ¹⁹J. P. Lu, J. B. Yau, S. P. Shukla, M. Shayegan, L. Wissinger, U. Rössler, and R. Winkler, Phys. Rev. Lett. **81**, 1282 (1998).
- ²⁰R. Winkler, S. J. Papadakis, E. P. De Poortere, and M. Shayegan, Phys. Rev. Lett. **84**, 713 (2000).